

PCCP

Accepted Manuscript



This is an *Accepted Manuscript*, which has been through the Royal Society of Chemistry peer review process and has been accepted for publication.

Accepted Manuscripts are published online shortly after acceptance, before technical editing, formatting and proof reading. Using this free service, authors can make their results available to the community, in citable form, before we publish the edited article. We will replace this *Accepted Manuscript* with the edited and formatted *Advance Article* as soon as it is available.

You can find more information about *Accepted Manuscripts* in the [Information for Authors](#).

Please note that technical editing may introduce minor changes to the text and/or graphics, which may alter content. The journal's standard [Terms & Conditions](#) and the [Ethical guidelines](#) still apply. In no event shall the Royal Society of Chemistry be held responsible for any errors or omissions in this *Accepted Manuscript* or any consequences arising from the use of any information it contains.

Ms: CP-ART-03-2015-001650 Revision 4 June 2015

Effects of Bimetallic Doping on Small Cyclic and Tubular Boron Clusters: B_7M_2 and $B_{14}M_2$ Structures with $M = Fe, Co$

Hung Tan Pham^{&, †} and Minh Tho Nguyen^{§,1}

[&] *Computational Chemistry Research Group, Ton Duc Thang University, Ho Chi Minh City, Vietnam*

[†] *Faculty of Applied Sciences, Ton Duc Thang University, Ho Chi Minh City, Vietnam*

[§] *Department of Chemistry, University of Leuven, B-3001 Leuven, Belgium*

Key Words:

Iron-doped boron tubes

Cobalt-doped boron tubes

Iron boron ring

Cobalt boron ring

Bimetallic Dopants

Electron Count Rules

¹ Email: minh.nguyen@chem.kuleuven.be

Abstract:

Using density functional theory with the TPSSh functional and the 6-311+G(d) basis set, we extensively searched for the global minima of two metallic atoms doped boron clusters B_6M_2 , B_7M_2 , $B_{12}M_2$ and $B_{14}M_2$ with transition metal element M being Co and Fe. Structural identifications reveal that B_7Co_2 , B_7Fe_2 and B_7CoFe clusters have global minima in a B-cyclic motif, in which a perfectly planar B_7 is coordinated with two metallic atoms placed along the C_7 axis. The B_6 cluster is too small to form a cycle with the presence of two metals. Similarly, the B_{12} cluster is not large enough to stabilize the metallic dimer within a double ring $2xB_6$ tube. The doped $B_{14}M_2$ clusters including $B_{14}Co_2$, $B_{14}Fe_2$ and $B_{14}CoFe$ have a double ring $2xB_7$ tubular shape in which one metal atom is encapsulated by the B_{14} tube and the other is located at an exposed position. Dissociation energies demonstrate that while bimetallic cyclic cluster B_7M_2 prefers a fragmentation channel that generates the B_7 global minimum plus metallic dimer, the tubular structure $B_{14}M_2$ tends to dissociate giving a bimetallic cyclic structure B_7M_2 and a $B@B_6$ cluster. The enhanced stability of the bimetallic doped boron clusters considered can be understood from the stabilizing interactions between the anti-bonding MOs of metal-metal dimers and the levels of a disk aromatic configuration (for bimetallic cyclic structures), or the eigenstates of the B_{14} tubular form (in case of bimetallic tubular structure).

1. Introduction

Boron-based systems have extensively been investigated with the aim of finding materials with novel structures and properties, and high thermodynamic stabilities. Of the pure boron nanostructures, the crystalline boron nanotube has recently been synthesized, and their electric transport properties are found to be close to those of the carbon nanotubes, irrespective

of their lattice structure and chirality.^{1,2,3} Regarding the molecular shape of boron clusters, the anions B_n^- possess the planar or quasi-planar form up to the size of $n \sim 25$,^{4,5,6} whereas the neutral counterparts going from $n = 20$ exhibit a variety of structures including quasi-planar, bowl-shaped, tubular, cage and fullerene-like shapes.⁷ While B_{20} has a double ring tubular structure,⁸ the B_{38} is considered as a critical size for 2D-3D structural transitions.⁹ The bowl-shaped B_{30} , B_{32} and B_{36} ^{10,11,12} and quasi-planar B_{35} ¹³ clusters can serve as building blocks to form various boron sheets. The finding of the triple ring B_{27}^+ ¹⁴ and B_{42} ¹⁰ tubes, structures formed by superposition of three B_9 and B_{14} strings in an anti-prism motif, respectively, illustrates that boron nanotubes can be constructed from small stable units. Let us note that in both B_{38} and B_{40} sizes, the fullerenes^{10,15} and the quasi-planar isomers⁹ are quite close in energy content. It should be stressed that the electronic structure of small sized boron clusters (B_n with n up to 20) can be rationalized using models of electron moving in different environments.^{16,17,18}

The boron atom has the capacity to form strong covalent bonds not only with itself but also with many other elements. Combined theoretical and experimental investigations revealed that the doping of transition metal elements on small boron clusters eventually lead to formation of the cyclic $M@B_n^{k-}$ structures in which the M atom is usually situated at the center of a B_n ring.¹⁹ Such a hypervalent structure was thus observed in many pure boron clusters involving the rings B_7^- , B_8 , B_8^{2-} and B_9^- .²⁰ The presence of negative charge is necessary to achieve planar structures. The central atom M tends to connect the B_n unit (anion or neutral molecule) through both delocalized π and σ bonds that are formed from interaction between the d -AO(M) and sp -AO(B), whereas the B-B bonds within the B_n ring are usually simple 2c-2e bonds. These cyclic structures are often regarded as having a double aromaticity involving both π and σ electrons, due to the fact that the number of each type of delocalized electrons satisfies the classical Hückel

$(4N + 2)$ electron count. A way of searching for new $M@B_n^{k-}$ rings is based on the electron requirement to form electronically stable and doubly aromatic cycles, in which the total $(3n + x + k)$ electrons participate in $n \times (2c-2e)$ B-B peripheral σ bonds and two sets of delocalized MOs (6σ and 6π electrons). Thus the electron count can be written as $3n + x + k = 2n + 12$. Such a design principle was successfully applied to boron rings with sizes of $n = 8$ and 9 including $Co@B_8^-$, $Fe@B_9^-$, $Ru@B_9^-$, $Rh@B_9$, $Ir@B_9$ ^{21,22}...

Several boron rings doped with other main group elements were theoretically searched, but none of them was found to be a global minimum on the corresponding potential energy surface.²³ The central atom M has to form delocalized π and σ bonds with the whole B_n skeleton, but when a main group element has a larger electronegativity, it favors connections through $2c-2e$ bonds. Geometric factors also play an important role in determining the global minima. Up to now, cyclic boron structures were not observed at the sizes $n < 8$, and for the sizes larger than $n > 10$ B atoms, the clusters tend to adopt leaf-like, pyramid-like and umbrella-like... structures.²⁴

Recently, we found that stabilized tubular and fullerene-type forms can be produced in boron clusters B_n from the sizes of $n \sim 14$ to 20 , following doping by an iron atom. Accordingly, the endohedrally Fe-doped boron clusters $B_{14}Fe$ and $B_{16}Fe$ are stable double ring tubes, whereas the $B_{18}Fe$ and $B_{20}Fe$ are stable fullerenes.²⁵ These represent the smallest tubular and fullerene-like forms of boron clusters. Their formation and high thermodynamic stability suggests the use of transition metal dopants to induce different growth paths leading to larger cages, fullerenes and tubes of boron.

As far as we are aware, investigation on multiply doped boron clusters was quite limited even though some boron compounds including two transition metal atoms were experimentally observed. The series of bimetallic Re complexes of boron was synthesized and structurally

characterized to be the triple-decker $[(\text{Cp}^*\text{Re})_2\text{B}_n\text{X}_n]$, with $n = 5-10$, $X = \text{H}$ or Cl and $\text{Cp}^* = \text{Me}_5\text{C}_5$, in which the B_nX_n rings were coordinated by two Re atoms. Among these Re-boranes, the B_5X_5 and B_6X_6 units were found to have perfectly planar pentagonal and hexagonal motifs, respectively.^{26,27} Recently the planar B_6 ring was found to play as a structural motif in the solid compound $\text{Ti}_7\text{Rh}_4\text{Ir}_2\text{B}_8$,²⁸ in which the B_6 unit is sandwiched by two Ti atoms.

In this context, it is legitimate to ask a question about the existence of other bimetallic cyclic structures in which a planar B_n ring encloses two metal atoms, in particular two different metals. The doping effect of such two metal atoms on the stability of tubular form of B_{2n} boron cluster is not well known yet. In order to tackle these issues, we set out to carry out a theoretical investigation on the doped series of B_nM_2 and B_{2n}M_2 both containing two transition metal atoms.

As in the case of singly-doped clusters B_nFe ,^{25,27} we found that both iron and cobalt elements, either 2Fe and 2Co or the mixed CoFe, exert a remarkable doping effects on the stability of the cyclic and tubular forms of boron clusters. With the aim of finding novel boron-based building-block nanostructures, we thus examine the doping behavior in the case of B_6M_2 , B_7M_2 , B_{12}M_2 and B_{14}M_2 clusters with M being the Fe and Co atoms and their mixture. It turns out that the $\text{Co}_2@\text{B}_7$, $\text{Fe}_2@\text{B}_7$ and $\text{CoFe}@\text{B}_7$ clusters are stabilized in a bimetallic-cyclic motif in which the perfectly planar B_7 is coordinated by two metallic atoms taken place along the C_7 axis, whereas the B_6 size is not able to form a cyclic motif with two metal elements.

Similarly, the B_{12} cluster is apparently not large enough to enclose the metallic dimer in a double ring form. The doped B_{14} clusters including $\text{Co}_2@\text{B}_{14}$, $\text{Fe}_2@\text{B}_{14}$ and $\text{CoFe}@\text{B}_{14}$ emerge with a bimetallic-axis tubular shape in which one metal atom is encapsulated by the double ring B_{14} tube, and the other is located outside. The metallic dimer consistently forms the axis of the highly symmetrical tube.

2. Computational Methods

Electronic structure theory computations are performed using the Gaussian 09 suite of program.²⁹ In this study, only density functional theory (DFT) methods are employed in the searches for equilibrium structures, and subsequent determinations of relative energies. Geometrical optimizations and harmonic vibrational calculations are carried out using the TPSSh functional³⁰ which was shown to give better results on relative energies for boron clusters than with other available functionals, as compared to the high accuracy MO coupled-cluster method (CCSD(T)).⁶ The search for global minima is conducted using the stochastic genetic algorithms to generate the possible initial structures.^{6,31} In addition, the guess structures are also manually built by adding two metal atoms to the framework of the pure B_n and B_{2n} hosts ($n = 6$ and 7). Initial structures are first optimized using the small 3-21G basis set.^{32,33} Selected lower-energy isomers, within a range of 50 kcal/mol on relative energies, are then reoptimized using the same functional but in conjunction with the larger 6-311+G(d) basis set.^{34,35} Unless otherwise noted, the relative energies mentioned hereafter are obtained from TPSSh/6311+G(d) computations. Energetic values are invariably referred to the energy of the corresponding global minimum. It is well known that relative energies obtained using DFT computations are strongly dependent on the functional employed. However, as stated above, the energy ordering of the isomers derived from the TPSSh functional for boron clusters can be compared with those obtained using CCSD(T) methods. We would expect an error margin of ± 4 kcal/mol or ± 0.2 eV on relative energies of cluster isomers, and ± 5 kcal/mol on dissociation energies. For the bare metallic dimers, the lower-lying spin state is determined using the TPSSh/6-311+G(d) theoretical level. The septet state is found as the ground state for Co_2 and Fe_2 dimers, while the sextet state turns out to be the lowest energy state of $CoFe$ (cf. Table 1). Accordingly, the TPSSh/6-311+G(d) level

reproduces well the spin states which agree with previous results obtained by CCSD(T)/cc-pVTZ-DK³⁹ and others DFT computations,^{40,41} namely a septet state for both Fe₂ and Co₂ and a sextet for CoFe dimer.

3. Results and Discussion

In the following sections, we will successively present the results for the B_nM₂ and then B_{2n}M₂ systems, with n being equal to 6 and 7. As for a convention, the structures reported are denoted by **nM₂.y**, in which **n** is the cluster size, namely n = 6, 7, 12 and 14, **M₂** = Co₂, Fe₂ and CoFe stand for two dopants, and finally **y** = 1, 2, 3,... label the isomers with increasing energy ordering. Let us mention that both 3d transition metals atoms have high spin ground states, Fe: [Ar] 3d⁶ 4s², ground state: ⁵D₄, and Co: ([Ar] 3d⁷ 4s², ground state: ⁴F_{9/2}. The shapes of the most stable isomers of bimetallic-doped B_nM₂ and B_{2n}M₂ with n = 6 and 7 are displayed in the Figure 1. To simplify the presentation of data, results of the extensive searches for bimetallic-doped B₆M₂, B₇M₂, B₁₂M₂ and B₁₄M₂ clusters are depicted in the Supplementary Information file (ESI).

3.1 Bimetallic Doped Clusters B₆M₂

B₆Co₂. TPSSh/6-311+G(d) + ZPE calculations point out that the high spin **6Co2.1** (C_s ⁵A'') and **6Co2.2** (D_{6h} ⁵A_{2u}) are competitive for the ground state, with a small energy gap of only 1 kcal/mol. **6Co2.1** is formed by capping a Co atom on the B₆ face giving a near-hexagonal B₆Co cyclic cluster (Figure 1a), whereas **6Co2.2** is actually generated by replacement of a B atom on the axis of the B₇Co global minimum, which also has a bi-pyramid shape.³⁶ Within the expected accuracy of DFT methods employed, both can be considered as energetically degenerate.

B₆Fe₂. The triplet **6Fe2.1** (C_s ³A''), a structure having a similar shape with the global minimum **6Co2.1** of B₆Co₂, is identified as the lowest-energy structure, but the corresponding quintet state is only at 2 kcal/mol higher in energy. It is thus not possible to firmly establish the ground state

of this cluster. Both spin states are likely to be nearly degenerate. The other low-lying isomers are shown in the Figure S1 of ESI.

B₆CoFe. Following the mixing of Fe and Co, the sextet bi-pyramid **6CoFe.1** (C_2 6A) isomer, a cyclic derivative in which Co and Fe are capped on two opposite sides of the B₆ plane is now located as the ground state. Due the asymmetry of the dopants, the resulting by-pyramid is getting slightly distorted along the molecular axis (Figure 1a). We refer to Figure S2 of the ESI for the low-lying isomers.

3.2 Bimetallic Doped Clusters B₇M₂: Stabilized Cyclic Members

B₇Co₂. Results of the search for global minimum of two-cobalt doped on the B₇ system are displayed in Figure 1b. The quartet heptagonal bi-pyramid **7Co2.1** (D_{7h} , $^4A''_2$) is identified as the ground state. This global minimum is again found to be in a seven-membered cyclic shape, in which two Co atoms coordinated in two opposite sides of the planar B₇ ring to form the highest point group of D_{7h} . Accordingly, both Co atoms form the C_7 axis and are sandwiched with a perfectly planar B₇ ring. For this structure, the doublet state is close to the quartet with a small D-Q energy gap of 4 kcal/mol. The most interesting finding is that the heptagonal bi-pyramidal quartet structure **7Co2.1** is beyond any doubt the most stable isomer of Co₂@B₇, and thus constitutes a new member of the bimetallic cyclic boron family.

B₇Fe₂. Similarly, the heptagonal bi-pyramid **7Fe2.1** (D_{7h} $^6A''_2$), possessing a sextet spin state, turns out to be the most stable isomer (Figure 1b). **7Fe2.1** is another cyclic boron structure, in which the dimer Fe₂ is symmetrically placed along the central C_7 axis of the planar B₇ ring. The higher energy isomers of B₇Fe₂ are displayed in the Figure S2 of ESI.

B₇CoFe. In the case the Co and Fe co-doping, the high spin and high symmetry heptagonal bi-pyramid **7CoFe.1** (C_{7v} $^5A''_2$) is calculated to be the most stable structure. It is thus unambiguous

that the **7CoFe.1** is a new bimetallic seven-membered cyclic motif containing two different metals. Results of the search for Co and Fe co-doped B_7 cluster are given Figure S2 of ESI.

3.3 Structure of Bimetallic Doped $B_{12}M_2$ Clusters

We now consider the sizes $2n = 12$ and 14 of B_{2n} clusters. The main purpose in selecting these specific sizes is to find out as to whether a tube superposing either two rings of B_6 or two rings of B_7 could be formed and stabilized. We consider in this section the $B_{12}M_2$.

$B_{12}Co_2$. The search for $B_{12}Co_2$ reveals that the triplet **12Co2.1** (C_s^3A''), which exhibits a strong distortion from a double ring tube surrounding the first Co atom, and the second Co atom is capped outside on a hexagonal face, is the most stable structure (Figure 1c). For this shape, the quintet state **12Co2.1** (C_s^5A'') is quite close to the triplet state, with an energy separation of 6 kcal/mol.

$B_{12}Fe_2$. For this di-iron doped cluster, there is also a competition for the ground state. Both quintet states **12Fe2.1** (C_s^5A'') and **12Fe2.2** (C_s^5A'') are equally stable with an energy separation of ~ 3 kcal/mol. As a consequence, they are competing for the ground state of $B_{12}Fe_2$.

$B_{12}CoFe$. Our extensive search for the structures of the mixed $B_{12}CoFe$ converges to the lowest-energy **12CoFe.1** (C_s^4A'') which possesses a similar shape as **12Co2.1** and **12Fe2.1** but with a quartet state (Figure 1c). The most characteristic feature of **12CoFe.1** is that the iron atom is capped outside on the hexagon, and the cobalt is inserted inside the tube surrounded by 12 B atoms.

3.4 Structure of Bimetallic Doped $B_{14}M_2$ Clusters

$B_{14}Co_2$. The extensive search for $B_{14}Co_2$ cluster using TPSSh/6-311+G(d) + ZPE computations points out that the high symmetry triplet **14Co2.1** ($C_{7v}^3A''_2$) is the ground state. This structure is composed of two seven-membered rings connected with each other in an anti-prism fashion. One

Co atom is doped at the central region, while the other is exposed outside the B₁₄ double ring. The double ring form exists in the di-cationic B₁₄²⁺ cluster and was considered as the smallest boron double ring tube.³⁷ The neutral B₁₄ was found to be stable in a fullerene-type form.³⁸ Our extensive calculations reveal that the doping of two Co atoms tends to stabilize more the double ring tubular structure than the fullerene.

B₁₄Fe₂. Both high spin states of the structure **14Fe2.1** having a similar shape to **14Co2.1** are competitive for the ground state. The quintet state **14Fe2.1** ($C_{7V} \ ^5A''_2$) and the triplet state **14Fe2.1** ($C_{7V} \ ^3A''_2$) possess comparable energy content, differ from each other by only ~2 kcal/mol. In contrast, the closed-shell singlet **14Fe2.1** ($C_s \ ^1A'$) is high in energy (56 kcal/mol).

B₁₄CoFe. The high symmetry quartet **14CoFe.1** ($C_{7V} \ ^4A''_2$) is once more identified as the ground state structure. This is a double ring tube characterized by the fact that the Co atom occupies the central position of the (2 x 7) B tube, and the Fe atom exohedrally caps on a B₇ face. **14CoFe.1** can be viewed as a particular situation of tubular type structure in which both metal nuclei form the C₇ axis and are half encompassed by a (2 x 7) B tube. A comparable structure in which the Fe is instead located at the central site of the B₁₄ double ring turns out to be highly unstable, and distorted into the **14CoFe.4**, which is 34 ($C_s \ ^6A''$), 16 ($C_s \ ^4A''$) and 18 ($C_s \ ^2A''$) kcal/mol higher than the ground state in all spin states (Figure S4 of ESI).

3.5 Geometric Requirements of Bimetallic Cyclic and Tubular Structures

After identifying the lowest-lying structures of the B_nM₂ and B_{2n}M₂ species, we now analyze the geometric requirements for formation of doped cyclic and tubular boron clusters. In general, a doubly doped **6M2.1** structure can be formed by adding a metal on the hexagonal face of the corresponding singly doped B₆M, which exhibits a hexagonal shape but with a B atom located at the central position.³⁹ The ground state of B₇M cluster has a bi-pyramid hexagonal

shape containing M-B C_6 axis. A replacement of the axial B atom by an M atom releases the **6M2.2** motif. As for a prediction, the B_8M cluster is expected to be stable in a bi-pyramid heptagonal shape with a M-B C_7 axis,³⁹³⁷ this is similar to the **7M2.1** structure in which the axial B atom replaced by the second metal. Accordingly, both minima **7M2.1** and **6M2.2** have a comparable motif of structure and are produced by a similar growth sequence. However **6M2.2** is competing with **6M2.1** for the global minimum status, whereas **7M2.1** is firmly the ground state. In other words, the B_6 ring is not favorable yet for formation of a bimetallic cycle. For the latter purpose, a B_7 ring more readily satisfies the geometric requirement.

For bimetallic doped $B_{12}M_2$ clusters, the **12M2.1** results from a strong distortion of a (2 x 6) B_{12} tube with one metal capped on the hexagonal face, but no tubular-type structure could be retained. In **12M2.2** which competes against **12M2.1** for ground state, the seven B atoms make a heptagonal face, and the five remaining B atoms cannot introduce the second ring but undergo a distortion giving rise to another hexagonal ring. No tubular structure can thus be formed. In view of the emergence of a heptagonal ring in **12M2.2**, the B_{14} system becomes significantly stabilized by the superposition of the second heptagon, and the most remarkable consequence is the production of a bimetallic double ring tube **14M2.1**.

3.6 Dissociation Energies

In order to better evaluate the stabilities of bimetallic doped boron clusters, the dissociation energies (DE) of various channels are computed and listed in Table 2.

The bimetallic doped B_6M_2 clusters prefer the dissociation pathway generating a metallic dimer plus B_6 cluster. A similar behavior is observed for B_7Co_2 , B_7CoFe and B_7Fe_2 cyclic structures, they favor the dissociation channel generating metal-metal dimers and $B@B_6$ structure.

For the bimetallic doped $B_{12}M_2$ clusters, the dissociation channel generating the global minimum of B_{12} plus metal-metal dimer is the most favored. The resulting pathway in which the parent clusters are fragmented into B_6 and the corresponding bimetallic doped B_6M_2 clusters is associated with much greater DE value, and thereby this channel is not opened.

The bimetallic-tubular structures of $B_{14}Co_2$, $B_{14}Fe_2$ and $B_{14}CoFe$ dissociate mainly through the channel generating the corresponding bimetallic cyclic form (B_7M_2) and $B@B_6$ cluster whereas the DE values of pathway resulting bimetallic cyclic structures (B_7M_2) and B_7 string are much higher, except for the case of $B_{14}CoFe$. Proceeding in the opposite direction, the bimetallic-tubular structure is a product of bimetallic cycle and $B@B_6$ cluster.

3.7 Chemical Bonding and Electron Shell Model

The stability of bimetallic-doped boron clusters can be understood in terms of electronic shell model. From the viewpoint of Jellium model,⁴⁰ which is successfully applied to interpret the stability of binary atomic clusters,^{41,42,43,44,45,46,47,48,49,50,51,52} the valence electrons are assumed to be freely itinerant in the spherical potential formed by the nuclei of atoms; the valence electrons will be occupied in the hydrogen-like orbitals with the pattern as $[1S^2 1P^6 1D^{10} 2S^2 1F^{14} 2P^6 1G^{18} 2D^{10} \dots]$. The number of electrons of 2, 8, 34, 40, 56, ... are magic numbers that actually correspond to a full filling of the successive electron shells, which ultimately leads to stable clusters.

The diagram of energy MO levels of B_7Co_2 and $B_{14}Co_2$ are given in Figure 2 and those of relevant clusters are given in the ESI file. In combining with the shape of MOs, the electron shells established for the clusters considered are listed in Table 3. Strong orbital overlaps between valence orbital located on metal (*sd*-AOs(M)) and valence orbital of B (*sp*-AOs(B)) appear to determine the shell configuration and induce the stabilities. The electrons of **6Co2.1** is

distributed in subshell of 1S, 1P, 1D, 2S, 2D and 2P with 28 electrons whereas in case of **6CoFe.1** and **6Fe2.1** 1F level appears beside 1P, 1D, 2S, 2D, 2P and 1F. All bimetallic doped B₇ clusters have the shell pattern occupied up to the 1F sublevel. As given in Table 3, the shell patterns assigned to B₁₂M₂ and B₁₄M₂ clusters are contributed by 1S, 1P, 1D, 1F, 1G, 2S, 2P and 2D subshells.

3.8 Orbital Interactions and Electron Counting for Bimetallic Cyclic and Tubular Structure.

3.8.1 The Co₂@B₇, Fe₂@B₇ and CoFe@B₇ Clusters. It is well known that the *d-d* interaction of two transition metal atoms usually give rise to a quadruple bond configuration such as: ($\sigma \pi \delta \delta^* \pi^* \sigma^*$).⁵³ The cobalt atom has an electron configuration of [Ar] 3d⁷ 4s², and as a consequence, the Co₂ dimer has enough electrons to fully occupy an electronic configuration of [$\sigma^2 \pi^4 \delta^4 \delta^{*4}$]. The Fe₂ dimer has a configuration of [$\sigma^2 \pi^4 \delta^4 \delta^{*2}$] from the shell structure of [Ar] 3d⁶ 4s² of Fe, and the mixed Co-Fe dimer contains 13 *d*-electrons filling up a configuration of [$\sigma^2 \pi^4 \delta^4 \delta^{*3}$]. In all cases, the anti-bonding δ^* MOs are filled and as a consequence, the strength of metal-metal bonding is reduced. In this section, we explore further the orbital interactions of metal dimers and B₇ and B₁₄ moieties.

The orbital interaction diagram between B₇ string and Co₂ is shown in Figure 3. For both Fe₂ and CoFe species, the corresponding diagrams are also given in Figures S7 and S8 of ESI. With an orbital configuration of B₇: [$1\sigma^2 2\sigma^2 1\pi^3$], the delocalized MO pattern of the B₇ string appears to satisfy a disk aromatic framework, which is raising, in term of irreducible representation, from a model of a particle in circular box.^{1644,1745,54} Within this model, the boundary condition gives rise to two quantum numbers, namely the radial quantum number *n* and the rotational quantum number *m*. These numbers have values *n* = 1, 2, 3, ... and *m* = 0, ±1, ±2, ... which is denoted as *m*

= σ , π , δ ,... respectively. A state with non-zero value of m is doubly degenerate. The lowest eigenstates in ascending energy are 1σ , 1π , 1δ ... *etc.* A full occupation of these eigenstates, both degenerate and non-degenerate, requires the amounts of 2, 6, 12, 16, 20,... electrons. These numbers are the characteristic electron counts of the disk aromaticity.

The fully occupied anti-bond δ^* MOs are stabilized upon interaction with the doubly degenerate vacant 1δ -MOs and produces the $1F_{23}$ subshell. The 2δ -MOs of B_7 string enjoy a stabilizing interaction with δ -MOs of Co_2 yielding the $2D_{xy}$ and $2D_{x^2-y^2}$ levels having similar irreducible representations to the δ level of a disk aromaticity framework. The anti-bonding π^* -MOs has a stabilizing interaction with the 1π level of B_7 and this gives rise to the $1D_{xz}$, $1D_{yz}$ and $2D_{xz}$, $2D_{yz}$ levels, in which the $1D_{xz}$ and $1D_{yz}$ levels have the same irreducible representation as the 1π state of the disk. The π bonding MOs of Co_2 have an enhanced overlapping with the 2π level of the B_7 disk generating the $2P_x$ and $2P_y$ levels (in terms of Jellium model) having the same node characteristics as the 2π levels.

Interaction of bonding σ MOs and the 2σ level ends up in the $1D_{z^2}$ and $2S$ subshells, where the $1D_{z^2}$ bears the same irreducible representation as the 2σ . Finally, anti-bonding σ^* -MO of Co_2 is stabilized upon interaction with the 1σ level of the B_7 disk, and yields the $1F_{23}$ subshell which is singly occupied. The anti-bonding MOs of Co_2 involving the δ^* , π^* and σ^* - MOs are significantly stabilized by overlapping with δ , π and σ levels of the B_7 disk including both empty and occupied MOs. On the basis of irreducible representation, a disk configuration is identified for $Co_2@B_7$ as $[1\sigma^2 1\pi^4 2\pi^4 1\delta^4 2\sigma^2 2\delta^4]$, in which the previously empty levels are filled, and this has a significant contribution to the overall stability.

Similar results are also obtained for B_7CoFe and B_7Fe_2 in which the anti-bonding MOs of $CoFe$ and Fe_2 species are greatly stabilized by interacting with the δ , π and σ levels of the B_7

disk. The disk aromatic configurations of $[1\sigma^2 1\pi^4 2\pi^4 1\delta^4 2\sigma^2 2\delta^3 \dots]$ and $[1\sigma^2 1\pi^4 2\pi^4 1\delta^4 2\sigma^2 2\delta^2]$ are thus identified for both B_7CoFe and B_7Fe_2 clusters, respectively.

3.8.2 Electron Counting. As the valence MOs of M_2 are formed from overlap of d -AOs, they could not interact with the states of disk model having rotational quantum number greater than 2. For this reason, the possible states of the B_7 disk which could overlap with M_2 species are the 1σ , 2σ , 1π , 2π , 1δ , and 2δ . Orbital interaction analysis illustrates that there are extra stabilizing interactions whose resulting MOs do not belong to the disk model (on the basis of irreducible representation). These extra interactions formed by overlapping π^* -MOs of metal-metal and 1π state of B_7 yield doubly degenerate $1D_{xz}$ and $1D_{yz}$ MOs which are occupied by 2 electrons in all cases, and maximum by 4 electrons. Combination of 2σ state and σ -MO turns out to give the $2S$ subshell fully filled by 2 electrons, whereas the 1σ and σ^* -MO interaction forms the $1F_{z^3}$ shell which is singly occupied in $Co_2@B_7$. Overall, the total number of electrons of a bimetallic cyclic structure includes the number of electrons occupied on the disk configuration plus the amount of electrons filled in extra MOs.

The B_7 string can introduce in total 21 valence electrons that are distributed in seven ($2c-2e$) bonds (14 electrons). The 7 remaining electrons are distributed in delocalized MOs. The M_2 unit gives x electrons, and thus the total number of electrons could be expressed as: $n + x = n(\text{disk}) + n(\text{extra})$, where $n(\text{disk})$ and $n(\text{extra})$ correspond to the number of electrons of the disk configuration and the extra stabilized MOs, respectively.

3.8.3 The $B_{14}Co_2$, $B_{14}Fe_2$ and $B_{14}CoFe$ Bimetallic Tubular Structures. The most recent investigation on of the tubular boron clusters B_{2n} , with $n = 10-14$, illustrates that the HOMOs can be classified into two distinct sets, namely the radial (r -MOs) and tangential (t -MOs) MO sets on the basis of the orientation of the p -lobes.⁵⁵ Another set of MOs is identified as s -MOs that are

constructed by a major contribution from *s*-AOs. The electron counting rule is in this case established as $(4N + 2M)$, with $M = 0$ and 1 , depending on the number of non-degenerate MO for both r-MOs and t-MOs sets.

In the case of tubular B_{14} structure, with $n = 7$, their MOs are also classified into three sets involving radial (r-MOs), tangential (t-MOs) and s-MOs sets. Let us now analyze orbital interactions of the t-MOs and r-MOs set of B_7 string with those of the metal-metal units.

3.8.4 Orbital Interaction of t-MOs Set and Co_2 , Fe_2 and $CoFe$. Interaction of the t-MOs set with the $[\sigma^2 \pi^4 \delta^4 \delta^{*4}]$ configuration of Co_2 is depicted in Figure 4. Combination of vacant $(3 \pm 2 1)$ MOs and the anti-bonding δ^* orbital (occupied by 4 electrons) creates some stable MOs, being identified as the $1G_{z^2}$ (x^2-y^2) and $1G_{xy^2}$ shells. This interaction introduces also doubly occupied MOs that are assigned by the $(3 \pm 2 1)$ level in terms of hollow cylinder model.⁴² The π^* MOs of Co_2 are stabilized by overlapping with the doubly occupied $(3 \pm 1 1)$ MOs of the double ring B_{14} , and form the $1F_{xz^2}$ and $1F_{yz^2}$ levels (fully filled by 4 electrons), and the doubly degenerate HOMO-1,1' subshell (occupied by 3 electrons).

The two shells $1F_{xz^2}$ and $1F_{yz^2}$, in terms of the Jellium model, also correspond to the doubly degenerate $(3 \pm 1 1)$ MOs of the hollow cylinder model. The weak interaction of the non-degenerate $(3 0 1)$ level and empty σ^* MO results in the $1F_{z^3}$ level. Similar results are obtained for the $B_{14}CoFe$ and $B_{14}Fe_2$ bimetallic tubular forms, as given in Figures S11 and S12 of ESI.

Orbital overlaps of the metallic dimer with the t-MO set of B_{14} tube end up in enhanced stability. Each of the bimetallic tube exhibits five fully filled MOs corresponding to the $(3 0 1)$, $(3 \pm 1 1)$ and $(3 \pm 2 1)$ states of the hollow cylinder model, thus satisfying the counting rule for tangential MO set with 10 electrons. In the case of $CoFe@B_{14}$, a singly occupied MO combining the $(3 0 1)$ level and σ^* -MO is identified. Due to the mixing of Co and Fe, a modification of the

potential occurs, and as a result, the energy ordering of the eigenvalues is changed.

3.8.5 Orbital Interaction of the r-MOs set with Co₂, Fe₂ and CoFe. Figure 5 displays the orbital interaction between MO(CO₂) and the radial MO set of the B₁₄ double ring, in which the δ*-MOs have no interaction. The lowest eigenvalue state of B₁₄ double ring (1 0 2) can only interact with the bonding and anti-bonding σ-MOs of M₂ to yield the 1D_{z²} and 2S subshells, respectively. The π*-MOs of Co₂ favorably overlap with the (1 ±2 2) eigenstates of B₁₄ and give rise to the 2D_{xz} and 2D_{yz} levels. Combination of π-MOs and (1 ±2 2) levels introduces the 2P_x and 2P_y subshells. The σ*-MO of Co₂ interacts with the doubly occupied state of (2 0 2) generates a fully filled MO which is assigned as the 2P_z subshell. Finally, the stability of δ bond is enhanced upon interaction with the empty (1 ±2 2) states of the double ring, and consequently produces the 2D_{x²-y²} and 2D_{xy} subshells. Similar orbital overlap patterns are also observed in the B₁₄CoFe and B₁₄Fe₂ tubular structure, as shown in Figure S9 and S10 of ESI.

The enhanced stability of bimetallic tubular clusters can thus in part be understood by introduction of M₂ dimer electrons to fill up the radial MOs (up to 11 electrons). The bare B₁₄ tube has only 8 radial electrons, populated in the (1 0 2), (1 ±1 2), (1 ±2 2) and (2 0 2) eigenstates. The anti-bonding MOs of M₂ are stabilized by interacting with the r-MOs set of the B₁₄ tube. The δ bond is reinforced in combining with the empty (1 ±2 2) level of the B₁₄ tube to yield the 2D subshell. We also note that the presence of transition metal dimers modifies the potential of hollow cylinder model, and as a consequence, the energy ordering of eigenstates can no longer be built as in the case of bare B_{2n} tubes.

3.8.6 Electron Counting Rule. Let us now analyse the electron counting for the M₂@B₁₄ tubular structures in the framework of the hollow cylinder model.^{14,61} Electron numbers for the r-MOs set are simply (4N), due to the fact that all structures considered have two non-degenerate MOs,

whereas those of the t-MOs set have $(4N+2)$ electrons. Because the MOs of M_2 are formed from d -AOs or sd -AOs, they can only interact with the MOs of the cylinder model having the quantum number l not greater than 2. On the other hand, all possible states of the r-MO set that can overlap with MOs of M_2 , include the levels of $(1\ 0\ 2)$, $(1\ \pm 1\ 2)$, $(1\ \pm 2\ 2)$, $(2\ 0\ 2)$, $(2\ \pm 1\ 2)$, $(2\ \pm 2\ 2)$... In the present case, 10 of the available electrons are found to be fully distributed in the $(1\ 0\ 2)$, $(1\ \pm 1\ 2)$ and $(1\ \pm 2\ 2)$ states, and the $(2\ 0\ 2)$ state is singly filled.

For the t-MOs set, only the $(3\ 0\ 1)$, $(3\ \pm 1\ 1)$ and $(3\ \pm 2\ 1)$ levels of the tube can interact with the MOs(M_2). They are fully occupied by 10 electrons and thus perfectly correspond to the $(4N + 2)$ counting rule (having no degenerate MOs). The special geometry in which one M atom is encapsulated inside the B_{14} double ring and the other is exposed outside, appears to be formed in order to gain stabilizing interactions of anti-bonding MOs of M_2 . The σ^* -MO and π^* -MO have the same irreducible representation to the $(1\ 0\ 2)$ and $(1\ \pm 1\ 2)$ MOs of the model, and consequently they induce extra interactions releasing the $2S$, $1F_{z-3}$, $2D_{xz}$ and $2D_{yz}$ levels. The latter are occupied by 8 electrons in the case of $Co_2@B_{14}$, but only 6 electrons for both $Fe_2@B_{14}$ and $CoFe@B_{14}$. The $1F_{z-3}$ subshell is not appeared in the latter cases.

Similar stabilizing interactions are also observed for the t-MOs set. Thus, interaction of the doubly degenerate π^* -MOs with the $(3\ \pm 1\ 1)$ state of the tubular-like B_{14} generates the doubly degenerate HOMO-1,1, which are occupied by 3 electrons in $Fe_2@B_{14}$ and $Co_2@B_{14}$ but 4 electrons in $CoFe@B_{14}$. The 4 electrons that induce extra stability, are distributed on both HOMO-2,2, and HOMO-1 of the mixed $CoFe@B_{14}$. Again, due to the involvement of extra MOs, an electron counting rule for all delocalized electrons cannot be established as in the bare B_{2n} tubes. For each MO set, a full electron occupation of the MOs of r-MOs or t-MOs sets induces extra stability.

3.8.7 Metal-Metal Bonding. It is now of interest to ask the question about the nature of the M-M bond. For this purpose, we consider the Mayer bond order (MBO) whose calculated values are given in Tables 4 and 5. The MBO of bare metallic dimers in the most stable spin state are given in Table 6. Metal-metal connections of B_nM_2 and $B_{2n}M_2$ clusters have values of MBO varying from 0.4 to 1.1, excluding the case of $B_{12}M_2$ being only 0.2. According to the usual meaning of bond order, such values illustrate the existence of direct metal-metal bonds with a single character. However, MBO values of doped boron are much smaller than that of bare dimeric metals (Table 6) while M_2 bond lengths of B_nM_2 and $B_{2n}M_2$ clusters are significantly larger than the isolated metallic dimers. As a result, B_n and B_{2n} counterparts reduce the bond order of dimeric metals and significantly increase the distance between two metal atoms.

3.8.8 Electron Localization Function Analysis. The electronic structure is further examined using the electron localization function (ELF). This partition of the density identifies the spaces of molecule where the electrons are present. The ELF maps of B_nCo_2 clusters are displayed in Figure 6, while the maps of others are shown in the Figure S13 of ESI. At high bifurcation value of 0.85, the ELF maps indicate a strong interaction between metallic dimers and boron framework. No localization domain can be observed between metal atoms and B_n counterparts, indicating a certain ionic feature of B-M bonds. The localization domain between two metal atoms can only be found at the low bifurcation value, even though the MBO values illustrate the single bond character for metal – metal moiety. The large radii of transition metals results in small concentration of electron density, and as a result the $V(M,M)$ basin can only be observed at small bifurcation values.

3.9 Forming Boron Tubes from Bimetallic Tubular Units.

In view of the tubular shape of the stable **14M2.1**, it is tempting to suggest that the

exohedral metal atom can serve as a linker which connects another $[B_{14}M]$ unit, with $M = Co$ and Fe , to form the doped boron tubes. Figure 10 depicts the optimized shapes of $B_{28}M_4$ structures produced by combination of two bimetallic tubular units (TPSSh/6-311+G(d) computations). The final configuration remains a tubular equilibrium structure. The transition metal atoms form the axis of the tube, whereas the merging of two B_{14} double rings ends up in a quadruple ring having the shape of the slightly distorted heptagonal tube. The persistence of an external metal atom following fusion of $[B_{14}M_2]$ units suggests that it plays the role of a linker allowing a continuing formation of a boron tube.

3.10 Vertical electron affinities (VEA) and vertical ionization energies (VIE).

The metal doped boron clusters can be determined experimentally comparing the vertical electron affinities (VEA) of the neutrals (detachment energies of the anions), or vertical ionization energies (VIE) of the neutrals, obtained from calculations and photoelectron spectroscopy. We determine here the VEA and VIE values for all neutral clusters considered. The VEA value is obtained from energy difference of neutral state and corresponding anion without structure optimization, while the VIE is calculated as energy difference between the neutral state and the cation having the neutral structure. As the B_nM_2 and $B_{2n}M_2$ clusters exhibit high spin state, the cationic and anionic states bear different multiplicities. Results of VEA and VIE are displayed in Tables 6 and 7. It appears that the VEA values are not quite large (~ 2 eV) and the VIE values are within the classical range of IEs of boron clusters.^{455†}

4. Concluding Remarks

We presented a theoretical investigation on the geometry, electronic structure and stability of B_6M_2 , B_7M_2 , $B_{12}M_2$ and $B_{14}M_2$ clusters involving a doping of two metal atoms Co and Fe . The bimetallic cyclic motif of structure is observed in the case of B_7Co_2 , B_7Fe_2 and B_7CoFe in which

perfect planar B_7 is coordinated by two metal atoms. On the contrary, the B_6 counterpart is not able to form a bimetallic cycle. The bimetallic doped $B_{12}M_2$ clusters are found to be stable with distorted double ring form, due to the fact that the B_{12} moiety is not large enough to result in a double ring motif.

The global minima of the two metal doped $B_{14}M_2$ clusters feature a tubular structure, in which one metal atom is encapsulated by B_{14} tube and the other is located outside. The two metal atoms form the C_7 axis of the tube. Dissociation energies illustrate that the $B_{14}Co_2$, $B_{14}Fe_2$ and $B_{14}CoFe$ bimetallic-tubular can be formed by combining the corresponding bimetallic cyclic and $B@B_6$ string.

The enhanced stability of bimetallic cyclic and tubular clusters can be understood from two perspectives: i) the anti-bonding and bonding MOs of metal-metal species induce stabilizing interactions with the levels of disk aromatic configuration (for bimetallic cyclic structures), and eigenstates of B_{14} tube (in case of bimetallic-tubular structure), and ii) both disk aromatic configuration and eigenstates of the hollow cylinder model gain more electrons due to a substantial electron transfer from dimeric metals. This induces a polarization of the metal dimer and some additional stabilizing electrostatic interactions.

In summary, we have found for the first time that the metal dimers such as Co_2 , Fe_2 , or $CoFe$ strongly stabilize the tubular form of boron clusters from a size as small as B_{14} . It is highly desirable to further investigate as to whether these bimetallic doped $B_{14}M_2$ could serve as realistic units for the generation of boron tubes.

Acknowledgements. We thank Ton Duc Thang University (TDT-DEMASTED) for support. MTN is indebted to the KU Leuven Research Council (GOA and IDO programs) for continuing

support.

Supplementary Information. Electronic file is available.

Table 1. The lower-lying spin states (multiplicity) of bimetallic species. Calculations were performed at the TPSSh/6-311+G(d) level. Relative energies (RE) are given in kcal/mol

Co ₂		Fe ₂		CoFe	
Multiplicity	RE	Multiplicity	RE	Multiplicity	RE
1	62	1	90	2	5
3	27	3	51	4	16
5	3	5	35	6	0.0
7	0.0	7	0.0	8	6
9	94	9	3	10	174
11	175	11	45	12	175

Table 2. The dissociation energies (kcal/mol) of bimetallic-doped B₇ and B₁₄ in various channels. Energy calculations were performed at the TPSSh/6-311+G(d) level.

Channel	Co	Fe	CoFe*
M ₂ B ₆ → M ₂ + B ₆	154.39	147.81	146.79
M ₂ B ₆ → 2M + B ₆	195.32	337.13	275.71
M ₂ ⊙B ₇ → B ₇ + M ₂	247.93	257.48	244.65
M ₂ ⊙B ₇ → B ₇ + 2M	288.85	446.80	373.56
M ₂ ⊙B ₇ → B⊙B ₆ + M ₂	160.20	169.75	156.92
M ₂ ⊙B ₇ → B⊙B ₆ + 2M	201.13	359.07	285.84
M ₂ B ₁₂ → B ₁₂ (opt) + M ₂	152.29	160.08	144.21
M ₂ B ₁₂ → B ₆ + M ₂ B ₆	235.48	249.85	235.00
M ₂ ⊙B ₁₄ → B ₁₄ + M ₂	233.70	241.44	224.22
M ₂ ⊙B ₁₄ → M ₂ ⊙B ₇ + B ₇	298.16	296.35	291.96
M ₂ ⊙B ₁₄ → M ₂ ⊙B ₇ + B⊙B ₆	210.43	208.62	204.23
M ₂ ⊙B ₁₄ → B ₁₄ (opt) + M ₂ (opt)	203.68	211.42	194.20

*in case of CoFe, M₂ stand for CoFe

Table 3. The shell configurations of the bimetallic doped boron clusters considered.

Species	Shell Configuration
6Co2.1	[1S ² 1P ² 1P ² 1D ² 1P ² 1D ² 2S ² 1D ² 1D ⁴ 2D ² 2P ² 2D ²]
6Fe2.1	[1S ² 1P ² 1P ² 1D ⁴ 1P ² 2S ² 1F ² 1D ² 1D ² 2P ² 2P ² 2D ²]
6CoFe.1	[1S ² 1P ⁴ 1D ⁴ 1P ² 1F ² 1F ² 1D ⁴ 2P ² 1F ² 1D ² 2P ² 2D ¹ 2D ¹ 2P ¹]
7Co2.1	[1S ² 1P ⁴ 1D ⁴ 1F ⁴ 1P ² 2S ² 2P ⁴ 1F ⁴ 1D ⁴ 1D ² 2D ⁴ 2D ³ 1F ¹]
7Fe2.1	[1S ² 1P ⁴ 1D ⁴ 1F ⁴ 1P ² 2S ² 2P ⁴ 1F ⁴ 1D ⁴ 1D ² 2D ³ 2D ²]
7CoFe.1	[1S ² 1P ⁴ 1D ⁴ 1F ⁴ 1P ² 2S ² 2P ⁴ 1F ⁴ 1D ⁴ 1D ² 2D ⁴ 2D ²]
12Co2.1	[1S ² 1P ⁶ 1D ⁶ 1F ² 1F ² 2S ² 1F ² 1F ² 1F ² 1G ² 1G ² 2D ² 2P ² 2D ² 1G ² 2D ² 3P ² 1G ² 2P ² 2P ¹ 1F ¹ ...]
12Fe2.1	[1S ² 1P ⁶ 1D ⁶ 1F ² 1F ² 2S ² 1F ² 1F ² 2S ² 1F ² 2P ² 2P ² 1F ² 2D ² 2D ² 3S ² 3P ² 1G ¹ 3P ¹ ...]
12CoFe.1	[1S ² 1P ⁶ 1D ⁶ 1F ² 1F ² 2S ² 1G ² 1F ² 1F ² 2P ² 2P ² 3S ² 1F ² 2D ² 2D ² 3P ² 3P ¹ ...].
14Co2.1	[1S ² 1P ⁴ 1D ⁴ 1P ² 1D ⁴ 1F ⁴ 1D ² 1F ⁴ 2S ² 1G ⁴ 1F ² 2D ⁴ 1F ⁴ 2D ⁴ 1G ⁴ 1G ⁴ 2P ¹]
14Fe2.1	[1S ² 1P ⁴ 1D ⁴ 1P ² 1D ⁴ 1F ⁴ 1D ² 1F ⁴ 2S ² 1F ² 1F ⁴ 1G ⁴ 2D ⁴ 1G ⁴ 2P ⁴ 1G ⁴ 2P ¹]
14CoFe.1	[1S ² 1P ⁴ 1D ⁴ 1P ² 1D ⁴ 1F ⁴ 1D ² 1F ⁴ 2S ² 1F ² 2D ⁴ 1G ⁴ 2D ⁴ 1F ⁴ 2P ⁴ 1G ⁴ 1G ³ 1G ¹ 2P ¹ ...]

Table 4. The Mayer bond order (MBO of M-M) and metal-metal bond length (Å) of bimetallic doped B_n and B_{2n} clusters with n = 6.

	Co ₂ B ₆	Fe ₂ B ₆	CoFeB ₆	Co ₂ @B ₁₂	Fe ₂ @B ₁₂	CoFe@B ₁₂
MBO	0.61	0.98	0.43	0.34	0.21	0.29
d(M-M)	2.45	2.46	2.72	2.52	2.66	2.58

Table 5. The Mayer bond order (MBO) and metal-metal bond length (Å) of bimetallic doped B_n and B_{2n} clusters with $n = 7$.

	$Co_2@B_7$	$Fe_2@B_7$	$CoFe@B_7$	$Co_2@B_{14}$	$Fe_2@B_{14}$	$CoFe@B_{14}$
MBO	0.81	1.1	0.54	0.44	0.47	0.46
d(M-M)	2.29	2.40	2.40	2.25	2.22	2.18

Table 6. The Mayer bond order (MBO) and bond length (Å) of metal dimers.

All values were calculated using the TPSSh/6-311+G(d) level.

	Co_2	Fe_2	$CoFe$
Multiplicity	7	7	6
MBO	2.6	3.1	1.7
d(M-M)	2.1	2.0	2.2

Table 7. Vertical electron affinities (VEA, eV) of B_nM_2 and $B_{2n}M_2$ clusters (TPSSh/6-311+G(d)).

	B_6M_2			B_7M_2		
	Co ₂	Fe ₂	CoFe	Co ₂	Fe ₂	CoFe
VEA1	1.43	1.74	-0.05	1.85	-0.69	8.86
VEA2	1.74	1.52	1.28	2.57	1.40	9.20
VEA3	1.74	1.89	1.80	1.71	2.04	9.12
	$B_{12}M_2$			$B_{14}M_2$		
	Co ₂	Fe ₂	CoFe	Co ₂	Fe ₂	CoFe
VEA1	0.83	1.02	1.16	0.34	-0.98	0.87
VEA2	2.17	2.14	2.47	1.79	1.71	1.79
VEA3	2.51	2.50	2.56	1.08	2.34	1.08

VEA1 = $E(B_nM_2) - (B_nM_2)^{\cdot-}$, singlet / doublet

VEA2 = $E(B_nM_2) - (B_nM_2)^{\cdot-}$ triplet / quartet

VEA3 = $E(B_nM_2) - (B_nM_2)^{\cdot-}$, quintet / sextet

Table 8. Vertical ionization energies (VIE, eV) of B_nM_2 and $B_{2n}M_2$ clusters (TPSSh/6-311+G(d)).

	B_6M_2			B_7M_2		
	Co ₂	Fe ₂	CoFe	Co ₂	Fe ₂	CoFe
VIE1	7.46	8.21	9.38	9.18	10.42	8.86
VIE2	7.57	7.19	7.76	8.73	8.26	9.20
VIE3	7.59	7.06	7.51	7.76	8.21	9.12
	$B_{12}M_2$			$B_{14}M_2$		
	Co ₂	Fe ₂	CoFe	Co ₂	Fe ₂	CoFe
VIE1	8.59	9.16	8.95	7.18	7.41	0.87
VIE2	7.85	7.86	7.81	7.18	7.21	7.16
VIE3	7.63	7.45	7.47	7.26	6.92	7.14

$$\text{VIE1} = (B_nM_2^+, \text{singlet / doublet}) - E(B_nM_2)$$

$$\text{VIE2} = (B_nM_2^+, \text{triple t/ quartet}) - E(B_nM_2)$$

$$\text{VIE3} = (B_nM_2^+, \text{quintet / sextet}) - E(B_nM_2)$$

Figure captions

Figure 1. The shapes of the global minima of B_nM_2 and $B_{2n}M_2$ clusters, with $n = 6$ and 7 . Geometry optimizations and energy calculations were performed using the TPSSh/6-311+G(d) level. a) B_6M_2 , b) B_7M_2 , c) $B_{12}M_2$ and d) $B_{14}M_2$, with $M = Co_2, Fe_2$ and $CoFe$. Green atom: Fe, Organ atom: Co and Red atom: B.

Figure 2. The diagram of energy MO levels of a) B_7Co_2 and b) $B_{14}Co_2$ (TPSSh/6-311+G(d)).

Figure 3. The diagram of orbital interactions between the B_7 disk and Co_2 dimer (TPSSh/6-311+G(d)).

Figure 4. Diagram of orbital interactions between the Co_2 dimer and the tangential MO set of B_{14} tube.

Figure 5. Diagram of orbital interactions between the Co_2 dimer and the radial MOs set of B_{14} tube.

Figure 6. The ELF iso-surfaces plotted at the bifurcation value of 0.85 of two Co doped B_n clusters, with $n = 6, 7, 12$ and 14 . Electron densities were obtained using TPSSh/6-311+G(d) computations.

Figure 7. Optimized structures of $B_{14}@Co-Co-Co@B_{14}$, $B_{14}Fe-Fe-FeB_{14}$, $B_{12}Fe-Co-FeB_{14}$ and $B_{14}Co-Fe-CoB_{14}$ (TPSSh/6-311+G(d)).

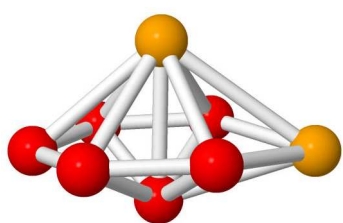
References

-
- 1 F. Liu, C. Shen, Z. Su, X. Ding, S. Deng, J. Chen, N. Xu and H. Gao, *J. Mater. Chem.* 2010, **20**, 2197.
 - 2 V. Bezugly, J. Kunstmann, B. G. Stock, T. Frauenheim, T. Niehaus and G. Cuniberti, *ACS Nano* 2011, **5**, 4997.
 - 3 D. Ciuparu, R. F. Klie, Y. Zhu and L. Pfefferle, *J. Phys. Chem. B* 2004, **108**, 3967.
 - 4 T. B. Tai and M. T. Nguyen, *Chem. Phys. Lett.* 2012, **530**, 71.
 - 5 A. P. Sergeeva, I. A. Popov, Z. A. Piazza, W. L. Li, C. Romanescu, L. S. Wang and A. I. Boldyrev, *Acc. Chem. Res.* 2014, **47**, 1349.
 - 6 H. T. Pham, L. V. Duong, B. Q. Pham and M. T. Nguyen, *Chem. Phys. Lett.* 2013, **577**, 32.
 - 7 T. B. Tai and M. T. Nguyen, *Phys. Chem. Chem. Phys.* 2015, **17**, 13672.
 - 8 B. Kiran, S. Bulusu, H. J. Zhai, S. Yoo, X. C. Zeng and L. S. Wang, *Proc. Natl. Acad. Sci. U.S.A.* 2005, **102**, 961.
 - 9 T. B. Tai and M. T. Nguyen, *Nanoscale* 2015, **7**, 3316.
 - 10 T. B. Tai, V. L. Duong, H. T. Pham, D. T. T. Mai and M. T. Nguyen, *Chem. Commun.* 2014, **50**, 1558.
 - 11 H. T. Pham, L. V. Duong, N. M. Tam, M. P. Pham-Ho and M. T. Nguyen, *Chem. Phys. Lett.*

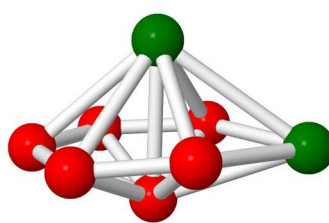
-
- 2014, **608**, 295.
- 12 T. B. Tai and M. T. Nguyen, *Chem. Commun.* 2015, **51**, 7677.
- 13 W. L. Li, Q. Chen, W. J. Tian, H. Bai, Y. F. Zhao, H. S. Hu, J. Li, H. J. Zhai, S. D. Li and L. S. Wang, *J. Am. Chem. Soc.* 2014, **136**, 12257.
- 14 L. V. Duong, H. T. Pham, N. M. Tam and M. T. Nguyen, *Phys. Chem. Chem. Phys.* 2014, **16**, 19470.
- 15 J. Lv, Y. Wang, L. Zhu and Y. Ma, *Nanoscale* 2014, **6**, 11692.
- 16 T. B. Tai, A. Ceulemans and M. T. Nguyen, *Chem. Eur. J.* 2012, **18**, 4510.
- 17 T. B. Tai, R. W. A. Havenith, J. L. Teunissen, A. R. Dok, S. D. Hallaert, M. T. Nguyen and A. Ceulemans, *Inorg. Chem.* 2013, **52**, 10595.
- 18 A. G. Arvanitidis, T. B. Tai, M. T. Nguyen and A. Ceulemans, *Phys. Chem. Chem. Phys.* 2014, **16**, 18311.
- 19 C. Romanescu, T. R. Galeev, W. L. Li, A. I. Boldyrev and L. S. Wang, *Acc. Chem. Res.* 2013, **46**, 350.
- 20 P. F. Fowler and B. R. Gray, *Inorg. Chem.* 2007, **46**, 2892.
- 21 Z. Pu, K. Ito, P. v. R. Schleyer and Q. S. Li, *Inorg. Chem.* 2009, **48**, 10679.
- 22 K. Ito, Z. Pu, Q. S. Li, P. v. R. Schleyer and Q. S. Li, *Inorg. Chem.* 2008, **47**, 10906.
- 23 Y. Liao, C. L. Cruz and P. v. R. Schleyer, Z. Chen, *Phys. Chem. Chem. Phys.* 2012, **14**, 14898.
- 24 I. A. Popov, W. L. Li, Z. A. Piazza, A. I. Boldyrev and L. S. Wang, *J. Phys. Chem. A* 2014, **118**,

-
- 8098.
- 25 N. M. Tam, H. T. Pham, L. V. Duong, M. P. Pham-Ho and M. T. Nguyen, *Phys. Chem. Chem. Phys.* 2015, **17**, 3000.
- 26 L. Guennic, H. Jiao, S. Kahlal, J. Y. Saillard, J. F. Halet, S. Ghosh, M. Shang, A. M. Beatty, A. L. Rheingold and T. P. Fehner, *J. Am. Chem. Soc.* 2004, **126**, 3203.
- 27 S. Ghosh, A. M. Beatty and T. P. Fehner, *J. Am. Chem. Soc.* 2001, **123**, 9188.
- 28 B. P. T Fokwa and M. Hermus, *Angew. Chem. Int. Ed.* 2012, **51**, 1702.
- 29 M.J. Frisch, H. B. Schlegel, G. E. Scuseria, M. A. Robb, J. R. Cheeseman, J. A. Montgomery, T. Vreven, K. N. Kudin, J. C. Burant, J. Millam, J. *et al.*, Gaussian 09 Revision: B.01; Gaussian, Inc.: Wallingford, CT, 2009.
- 30 J. M. Tao, J. P. Perdew, V. N. Staroverov and G. E. Scuseria, *Phys. Rev. Lett.* 2003, **91**, 146401.
- 31 T. B. Tai and M. T. Nguyen, *J. Chem. Theoret. Comput.* 2011, **7**, 1119.
- 32 M. S. Gordon, J. S. Binkley, J. A. Pople, W. J. Pietro and W. J. Hehre, *J. Am. Chem. Soc.* 1983, **104**, 2797.
- 33 K. D. Dobbs and W. J. Hehre, *J. Comput. Chem.* 1987, **8**, 861.
- 34 K. Raghavachari, J. S. Binkley, R. Seeger, and J. A. Pople, *J. Chem. Phys.*, 1980, **72**, 650.
- 35 P. J. Hay, *J. Chem. Phys.*, 1977, **66**, 4377.
- 36 X. Liu, G. F. Zhao, L. J. Guo, Q. Jing and Y. H. Luo, *Phys. Rev. A* 2007, **75**, 063201.
- 37 Y. Yuan and L. Cheng, *J. Chem. Phys.* 2012, **137**, 044308.
- 38 L. Cheng, *J. Chem. Phys.* 2012, **136**, 104301.

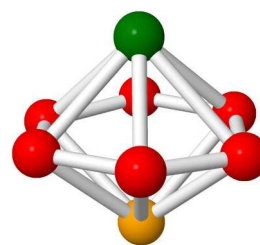
-
- 39 Z. Yang and S. J. Xiong, *J. Chem. Phys.* 2008, **128**, 184310.
- 40 M. Brack, *Rev. Mod. Phys.* 1993, **65**, 67.
- 41 V. T. Ngan and M. T. Nguyen, *J. Phys. Chem. A* 2010, **114**, 7609.
- 42 T. B. Tai and M. T. Nguyen, *J. Phys. Chem. A* 2011, **115**, 9993.
- 43 T. B. Tai and M. T. Nguyen, *Chem. Phys. Lett.* 2010, **492**, 290.
- 44 T. B. Tai, H. M. T. Nguyen and M. T. Nguyen, *Chem. Phys. Lett.* 2011, **502**, 187.
- 45 T. B. Tai, N. M. Tam and M. T. Nguyen, *Chem. Phys.* 2011, **388**, 1.
- 46 M. B. Abreu, A. C. Reber and S. N. Khanna, *J. Phys. Chem. Lett.*, 2014, **5**, 3492.
- 47 R. B. King, I. Silaghi-Dumitrescu and M. M. Uță, *Inorg. Chem.*, 2009, 48, 8508.
- 48 X. Huang, H.-G. Xu, S. Lu, Y. Su, R. B. King, J. Zhao and W. Zheng, *Nanoscale*, 2014, 6, 14617.
- 49 E. N. Esenturk, J. Fettinger and B. Eichhorn, *J. Am. Chem. Soc.* 2006, 128, 9178.
- 50 M. M. Uță, D. Cioloboc, and R. B. King, *J. Phys. Chem. A*, 2012, 116, 9197.
- 51 P. Pykkö and N. Runeberg, *Angew. Chem. Int. Ed.* 2002, 41, 2174
- 52 V. M. Medel, A. C. Reber, V. Chauhan, P. Sen, A. M. Köster, P. Calaminici and S. N. Khanna, *J. Am. Chem. Soc.*, 2014, **136**, 8229.
- 53 F. A. Cotton and D. G. Nocera, *Acc. Chem. Res.* 2000, **33**, 483.
- 54 T. B. Tai, V. T. T. Huong and M. T. Nguyen, *Top. Heterocyc. Chem.* 2014, **38**, 161.
- 55 H. T. Pham, V. L. Duong and M. T. Nguyen *J. Phys. Chem. C* 2014, **118**, 24181.



6Co2.1
 $C_s^5 A''$

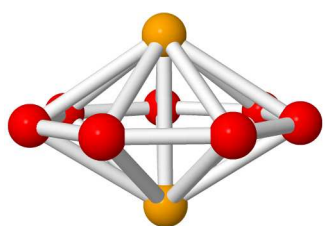


6Fe2.1
 $C_s^3 A''$

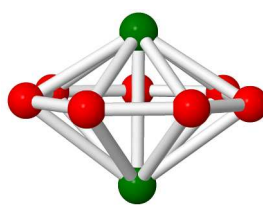


6CoFe.1
 $C_2^6 A$

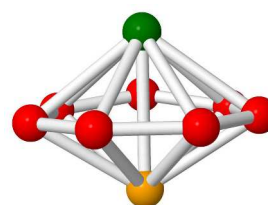
a)



7.Co2.1
 $D_{7h}^6 A''_2$

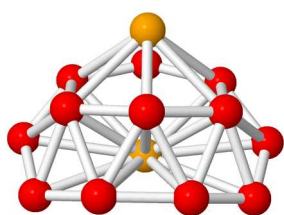


7.Fe2.1
 $D_{7h}^6 A''_2 0.0$

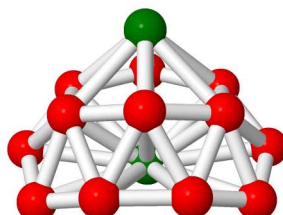


7.CoFe.1
 $C_{7v}^5 A''_2$

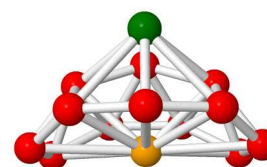
b)



12Co2.1
 $C_s^3 A''$

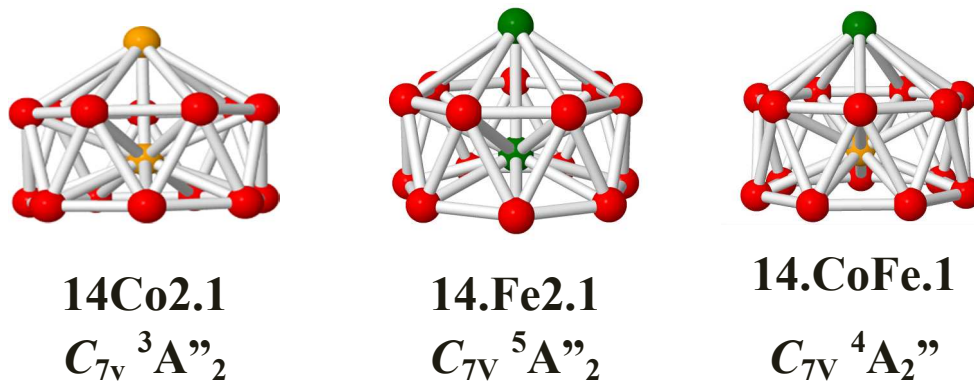


12Fe2.1
 $C_s^5 A''$



12CoFe.1
 $C_s^4 A''$

c)



d)

Figure 1.

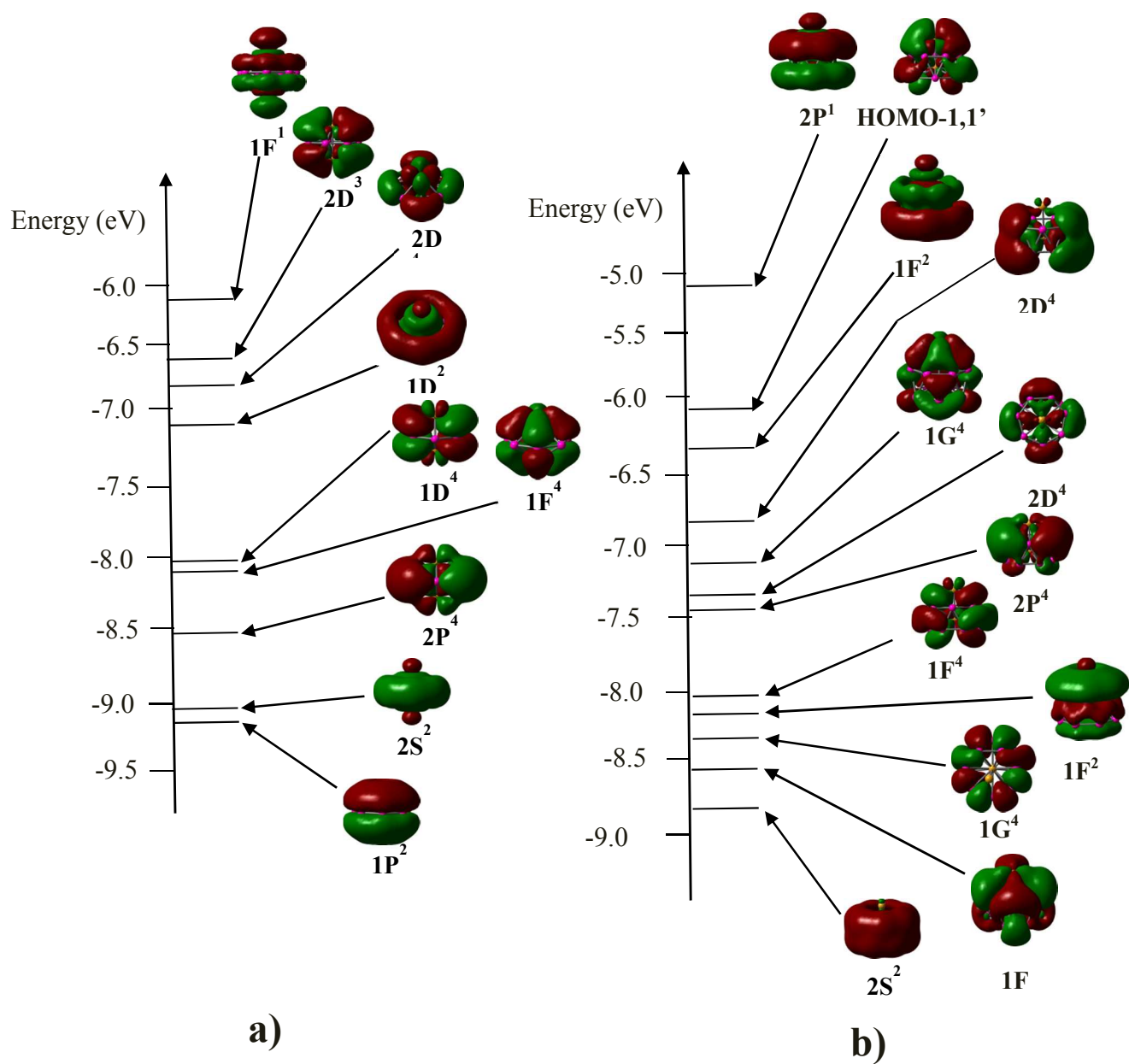


Figure 2

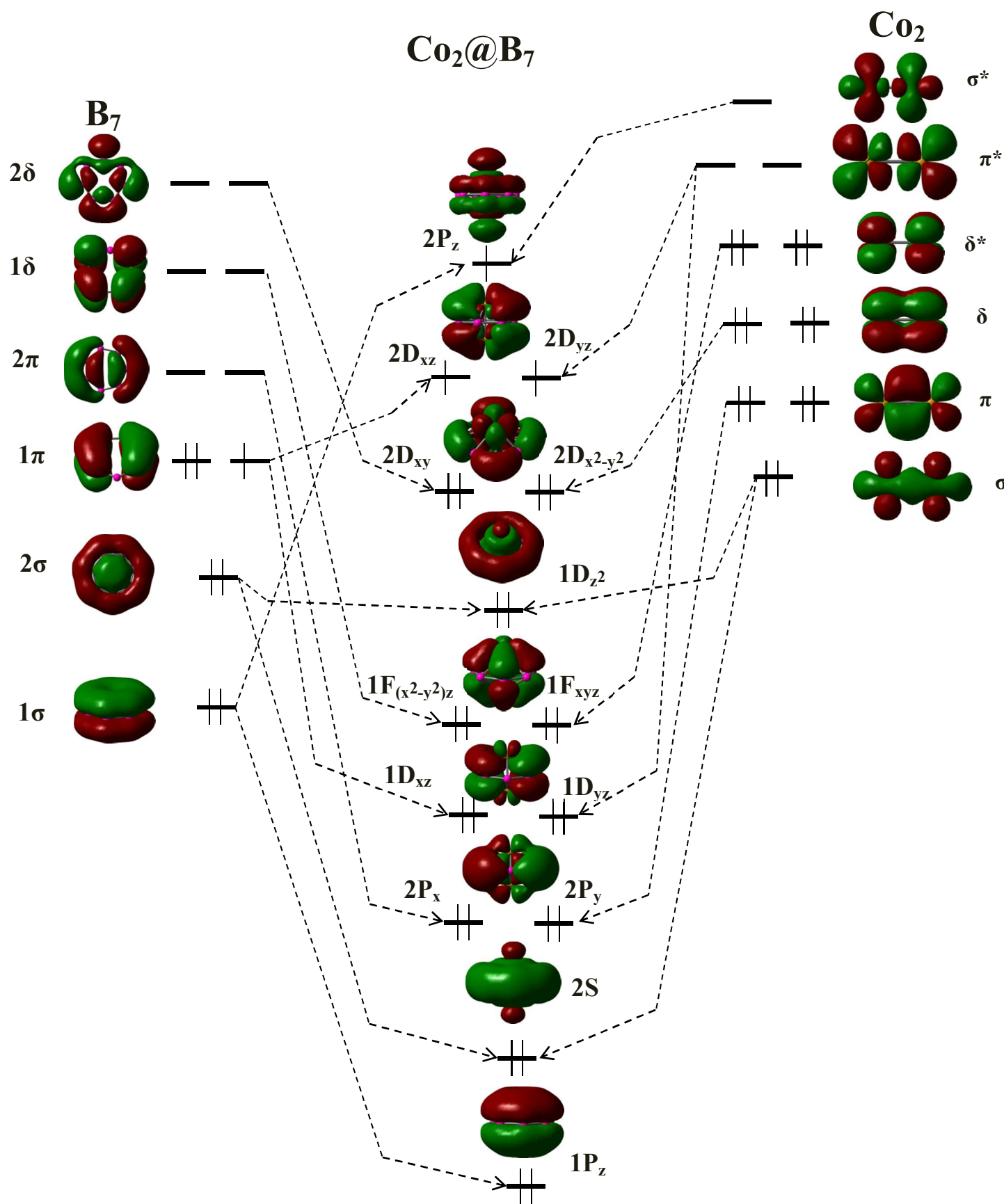


Figure 3.

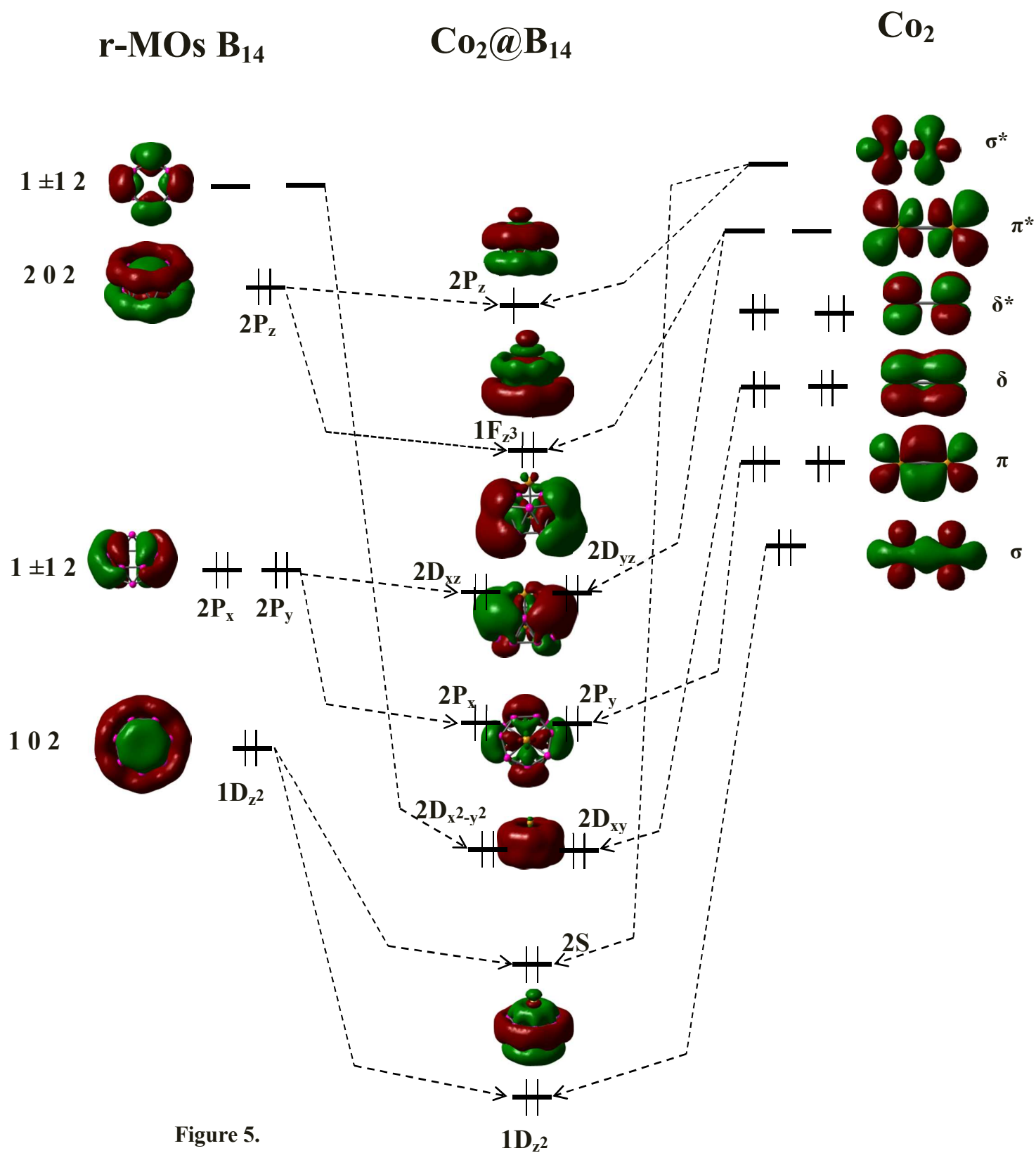


Figure 5.

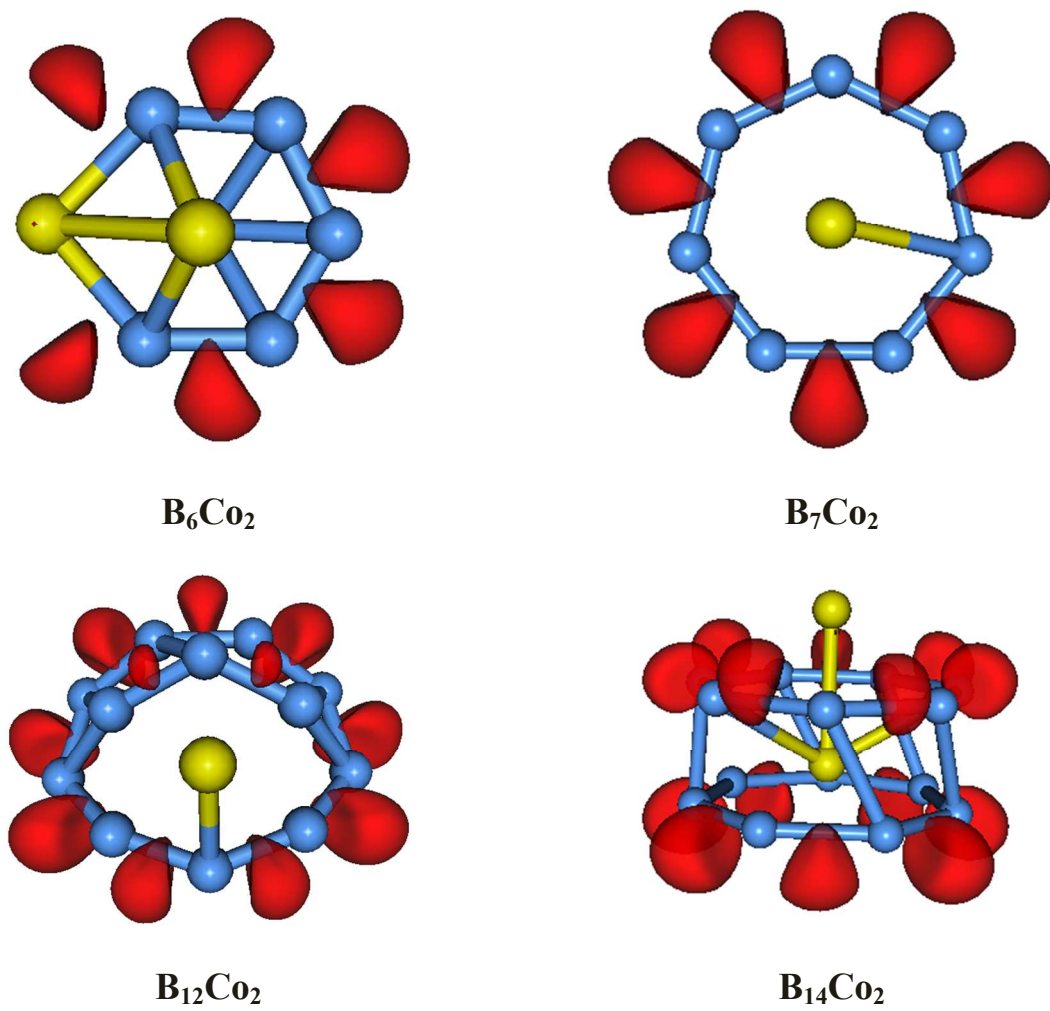


Figure 6.

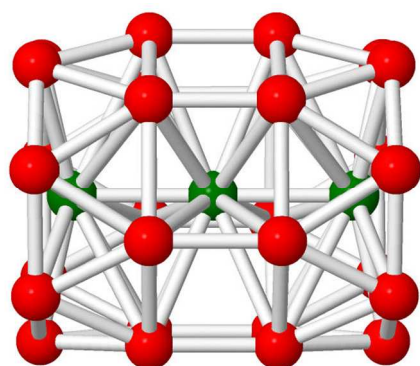
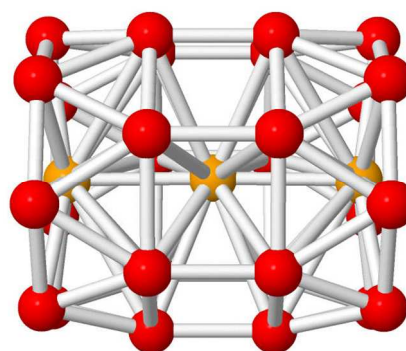
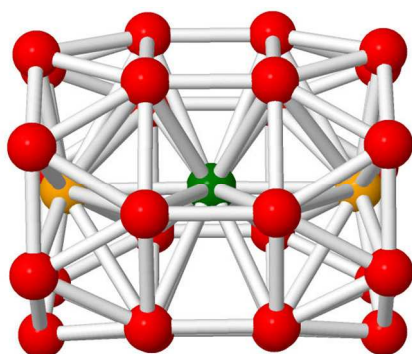
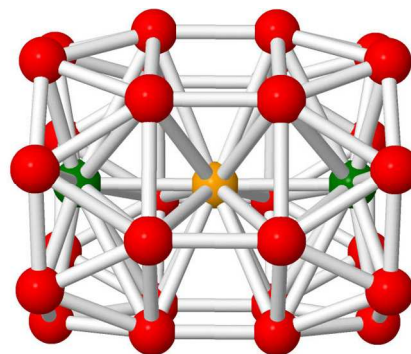
 $B_{14}Fe-Fe-FeB_{14}$  $B_{14}Co-Co-CoB_{14}$  $B_{14}Co-Fe-CoB_{14}$  $B_{14}Fe-Co-FeB_{14}$

Figure 7.